IMECE2008-68854

AUTOMATED WELD DEFECTS DETECTION USING IMAGE PROCESSING AND CAD METHODS

Reza Nejatpour
Department of Mechanical Engineering
Ferdowsi University of Mashhad
Mashhad, Iran
nejatpoor@gmail.com

Ali Asmari Sadabad
Department of Mechanical Engineering
Ferdowsi University of Mashhad
Mashhad, Iran
ali.asmari@gmail.com

Ali Akbar Akbari
Department of Mechanical Engineering
Ferdowsi University of Mashhad
Mashhad, Iran
a.a.akbari@um.ac.ir

ABSTRACT

One of the simple, fast, and economical methods for controlling the condition of a weld is checking its superficial appearance. In this paper a method, based on the composition of Image Processing and CAD algorithms is presented for controlling different welding defects. The main purpose of this project is omission of the human interference in Visual Test of the weld. The main core of this system is a computer which analyses the captured images of a CCD camera and extracts the parameters of the weld such as size, position, surface smoothness and etc. By putting the results of analyses executed on the images captured from different sections of the weld next to each other, a continuous, 3D model of the weld is achieved. By comparison of this model with the standard samples, the probable defects on the weld and the type of each recognized defect is defined. Omission of human mistakes, decrease in the costs, higher speed of the control line and coincidence with the new production standards are the advantages of this method. The presented method has been implemented on the automobile rings manufactured in Mashhad Wheel Manufacturing Co.
Keywords: Image Processing, Visual Test, Weld Defect

INTRODUCTION

Seam welding is one of the most important processes in manufacturing. Because of the high temperature and various welding situations the process is naturally complicated and nonlinear which makes the prediction of the result impossible [1]. So in order to avoid any failure in the final products, welding results always require quality control.

Detection and correction of the defects is a very time and cost consuming process for the manufacturers. There are many non destructive methods for detecting weld defects. Radiographic tests, ultrasonic sensors and magnetic sensors are of these kinds [2]. None of these methods can detect all kind of weld defects. And among them visual tests has many capabilities, and its main advantage is its simplicity and rapidity. In this method the operator observes different weld parameters such as weld position, weld length, and weld width, continuity of the weld strip and possible porosity along the weld.

Expert operators are the basis of this method. But development of science and technology along with the generative need of industry has encouraged the engineers to represent new ideas and methods for detecting weld defects. These methods not only increase the accuracy and the speed of the control process but also decrease the costs of production. The reliability of the products in this method is more and their quality is more coincident with standards [9].

1

In the first part of this paper the presented method is described. In the second section the method for dimension derivation is represented. The weld model generation using the derived dimensions is described in the third part. The fourth part is about defect detection from the generated model of the weld. At the end of this paper with discuss on the results and the proposed method.

METHOD DESCRIPTION

Confidence on the product quality in the production process and detecting the defects on the surface of the pieces such as cracks and corrosions are the example of visual tests usages [11]. Using this method we can find surface defects and irregularities on the parts. These methods because of their simplicity, fast procedures and low costs have been used in a wide range of applications. Using visual test we can survey general situations of a part. The main problem with this method is the necessity of the presence of a trained operator which often follows many problems such as:

1- Necessity of the presence of a full time operator
2- Its harmful effects on the health of the operator
3- Effect of operator's self discretion on the final decision
4- Low speed
5- Human mistakes

The quality of a good and appropriate weld can be recognized from different elements such as strength, external appearance, withstand against fatigue and etc. Size of the spot, the position of the weld and its structure are some of the main parameters in weld defects detection using visual tests. So for having a precise survey all of these parameters should be extracted. In this project for extracting different parameters of weld spot we have used a method based on the composition of image processing methods and CAD algorithms. The project has two main parts, extracting weld model from the images and then comparison of this model by a reference model which is acceptable and detecting the possible defects. In model extraction part we first radiate a laser beam on a section of the weld. Its projection is then captured with a CCD camera and transferred to a computer. In the computer the image processing operators are applied to the images and the profile of the section is extracted. Using a calibration matrix we convert this segment of points to a matrix of dimensions. Afterwards a B-Spline curve is fitted on the extracted segment which contains all of the numeral parameters this section of the weld spot. Depth, size and the quality of the section of the weld can be calculated from this matrix. Figure 1 shows a schematic view of this method.
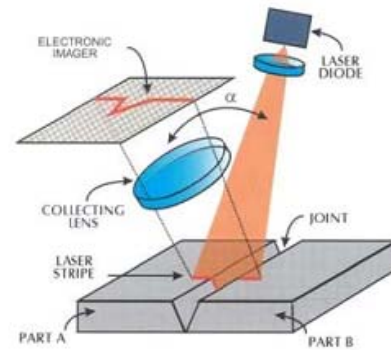

Figure 1 - schematic view of extracting the image of a section

In order to survey other defects of the weld spot, calculating its length and exact location is necessary. So the weld is observed in different and consecutive sections. In this method the welded part rotates about an axis and the images are captured from different sections of the weld spot. By succession of these sections we generate a 3D model of the weld spot. Figure 2 shows 3 samples captured from different sections of a weld spot.
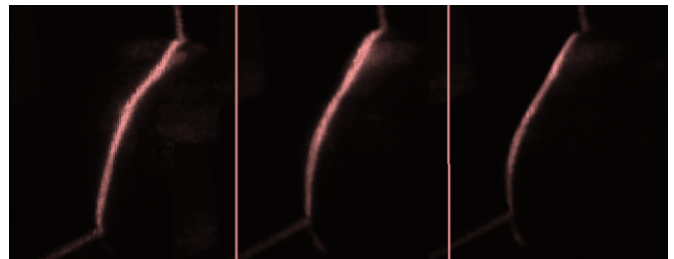

Figure 2 - 3 samples of the images captured from different sections of a weld spot

The generated model is then compared with a reference sample and other weld defects like defects in the length of the weld spot or its location, if any can be recognized.

DIMENSION EXTRACTION FROM IMAGES

Extracting dimensions from the image requires consumption of special mathematical methods called camera calibration [3]. Calibration is a conversion which correlates a point in the 3D coordinate with its match point in the plane of the image. In order to calculate the calibration matrix, internal specifications of the camera like numeral specifications and optical specifications and external specifications like camera position and orientation should be encountered [4].

For calculating the values of the calibration matrix we have used the pinhole camera model. This model is based on the light locomotion in the straight line. In this model any point in the coordinate of the object is connected to a point in the planar coordinate of the image with a straight line. Figure 3 shows how a point in the 3D coordinate is correlated to its projection in the plane of the image.
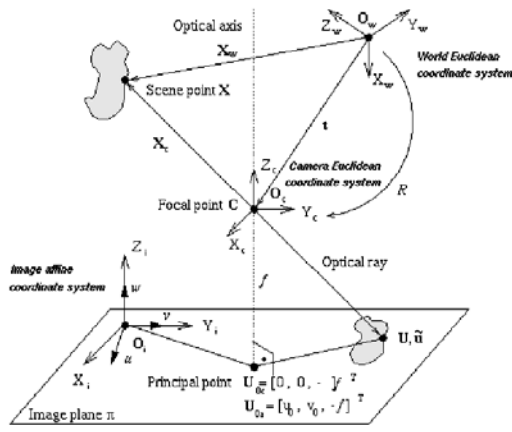
Figure 3 - correlation of points to their image in the pinhole camera model

In this model the coordinates of the camera is located in the center of transmission regarding the coordinates of the part (Xo, Yo, Zo) and the axis of the camera coordinate is perpendicular with the axis of the coordinate of the part. For representing the rotation equations of the axis we have used the equations of Euler's degrees. Transmitting a desired point P defined by (Xi, Yi, Zi) from the 3D coordinates C to the coordinates of the camera requires a rotation and a transmission. So we have:

$$\begin{bmatrix} x_i \\ y_i \\ z_i \end{bmatrix} = \begin{bmatrix} m_{11} & m_{12} & m_{13} \\ m_{21} & m_{22} & m_{23} \\ m_{31} & m_{32} & m_{33} \end{bmatrix} \begin{bmatrix} X_i \\ Y_i \\ Z_i \end{bmatrix} + \begin{bmatrix} x_0 \\ y_0 \\ z_0 \end{bmatrix} \tag{1}$$

This transmission has 6 degrees of freedom, 3 of which belong to rotation and the other 3 degrees of freedom belong to the transmitting matrix. Transmitting point P from the coordinate of the part to the coordinate of the image also depends on the camera specifications, such as focus distance of the lens, ratio of the length of the image in horizontal direction to the vertical direction *"Su"* and the center of the image *(U0, V0)*. For converting the metric dimensions to pixel calculating the constants *Du* and *Dv* are necessary. Because these constants depend linearly on *f* and *Su*, we can calculate them from *f* and *Su*. For converting the dimensions of point *P* from the coordinates of the camera to the coordinates of the image we can use equation (2).

$$\begin{bmatrix} \tilde{U}_i \\ \tilde{V}_i \end{bmatrix} = \frac{f}{z_i} \begin{bmatrix} x_i \\ y_i \end{bmatrix} \tag{2}$$

These equations show the dimensions in metric units. So for converting them to pixel units we use equation (3)

$$\begin{bmatrix} U'_i \\ V'_i \end{bmatrix} = \begin{bmatrix} D_U S_U \tilde{U}_i \\ D_V \tilde{V}_i \end{bmatrix} + \begin{bmatrix} U_0 \\ V_0 \end{bmatrix} \tag{3}$$

The pinhole camera model is a good approximation for representing the process of image constitution which simplifies the mathematical equations and is always valid in most of the applications, except in very accurate applications. In the exceptions it is also used as the base model and for correcting the unevenness of the image in some areas, some correction coefficients are applied.

In most of the cases the physical characteristics of the camera are not regarded. And the calibration matrix values are calculated using algebraic equations on some specific points. Using a transmission matrix the dimensions of the points are converted from the coordinates of the part (Xi, Yi, Zi) to the coordinates of the image (Ui, Vi). Equation (4) shows this transmission.

$$[U] = [A][X]$$

$$\begin{bmatrix} u_i w_i \\ v_i w_i \\ w_i \end{bmatrix} = \begin{bmatrix} a_{11} & a_{12} & a_{13} & a_{14} \\ a_{21} & a_{22} & a_{23} & a_{24} \\ a_{31} & a_{32} & a_{33} & a_{34} \end{bmatrix} \begin{bmatrix} X_i \\ Y_i \\ Z_i \\ 1 \end{bmatrix} \tag{4}$$

For calculating the twelve unknowns a_{ij} we need the dimensions of at least twelve points in coordinates of the part and the corresponding dimensions in the coordinates of the image. By omission of *wi* from the above equation the following equations are derived.

$$L = \begin{bmatrix} X_1 & Y_1 & Z_1 & 1 & 0 & 0 & 0 & 0 & -X_1 u_1 & -Y_1 u_1 & -Z_1 u_1 & -u_1 \\ 0 & 0 & 0 & 0 & X_1 & Y_1 & Z_1 & 1 & -X_1 v_1 & -Y_1 v_1 & -Z_1 v_1 & -v_1 \\ \vdots & \vdots & \vdots & \vdots & \vdots & \vdots & \vdots & \vdots & \vdots & \vdots & \vdots & \vdots \\ X_i & Y_i & Z_i & 1 & 0 & 0 & 0 & 0 & -X_i u_i & -Y_i u_i & -Z_i u_i & -u_i \\ 0 & 0 & 0 & 0 & X_i & Y_i & Z_i & 1 & -X_i v_i & -Y_i v_i & -Z_i v_i & -v_i \\ \vdots & \vdots & \vdots & \vdots & \vdots & \vdots & \vdots & \vdots & \vdots & \vdots & \vdots & \vdots \\ X_N & Y_N & Z_N & 1 & 0 & 0 & 0 & 0 & -X_N u_N & -Y_N u_N & -Z_N u_N & -u_N \\ 0 & 0 & 0 & 0 & X_N & Y_N & Z_N & 1 & -X_N v_N & -Y_N v_N & -Z_N v_N & -v_N \end{bmatrix} \tag{5}$$

$$a = \begin{bmatrix} a_{11} & a_{12} & a_{13} & a_{14} & a_{21} & a_{22} & a_{23} & a_{24} & a_{31} & a_{32} & a_{33} & a_2 \end{bmatrix} \tag{6}$$

$$La = 0 \tag{7}$$

By using the dimensions of the points in the image and their corresponding dimensions in the 3D coordinates the values of a_{ij} are calculated. To avoid the evident result $a_{ij} = 0$ the constraint $a_{31}^2 + a_{32}^2 + a_{33}^2 = 1$ is suggested.

3

In the specific situation in which all of the points of the part are in a plane, the constants a_{13}, a_{23} and a_{33} are multiplied by $z=0$. So the number of unknowns is reduced to 9 and equation (4) in simplified as follows:

$$\begin{bmatrix} u_i w_i \\ v_i w_i \\ w_i \end{bmatrix} = \begin{bmatrix} a_{11} & a_{12} & a_{13} \\ a_{21} & a_{22} & a_{23} \\ a_{31} & a_{32} & a_{33} \end{bmatrix} \begin{bmatrix} X_i \\ Y_i \\ 1 \end{bmatrix} \qquad (8)$$

To avoid the evident result $a_{ij}=0$ the constraint $a_{33}{}^2 = 1 - (a_{11}{}^2 + a_{32}{}^2)$ is suggested. By using this equation the number of unknowns is reduced to 8. In order to find these unknowns we need the dimensions of 4 points in the 3D coordinate of the part and their corresponding dimensions in the coordinates of the image.

These points are defined using gages with specific dimensions as shown in figure (4). The figure shows a 12*12*12mm gage on which a laser beam is projected. The incidence point of the laser beam and the edges of the gage are specified by markers.
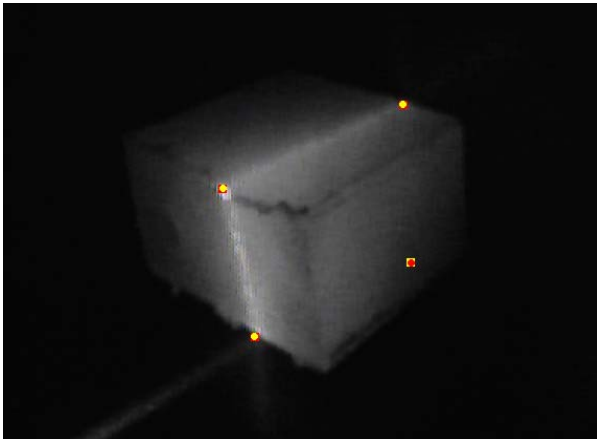

Figure 4 – a gage on which a laser beam is projected

Using these points we calculate the calibration matrix with which we can calculate the dimension of the points in the image.

SECTION COMPUTATION

A rescaled view of a section of the weld on which laser beam is projected is shown in figure 5. For extracting the weld section from this image there are standard methods in digital image processing which has been discussed in edge detection section.
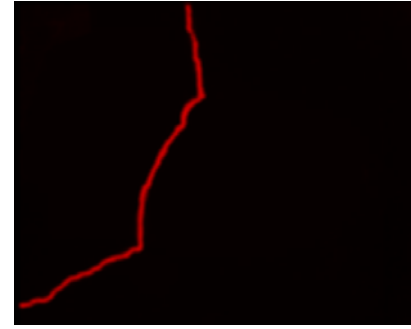

Figure 5 – projection of laser beam on the weld section

Edge detection result is a binary matrix in which the points on the edges are 1 and it's other points are 0. But because of the various electrical, magnetic and optical effects, the image captured from the camera has too many noises. And edge detection on these image increases the effects of these noises which may influence the accuracy of the method in the next steps. In order to decrease these noises we have used the Gaussian Median Filter. By consuming the image as a continuous and 2D function, *f(x,y)*. Equation (9) shows the general matrix *G(x,y)*, resultant of applying Gaussian Filter.

$$G(x,y) = \frac{1}{2\pi\sigma^2} e^{-\frac{x^2+y^2}{2\sigma^2}} \qquad (9)$$

This equation shows the general form of the Gaussian Filter in the continuous 2D plane, in which σ is the paragon deviation. In the discontinuous plane this filter is approximated by a 2D matrix. In this case for simplicity of the equations we have approximated the filter with a 5*5 matrix. Equation (10) shows this matrix.

$$G_{5\times5} = \begin{bmatrix} 0.003 & 0.0133 & 0.0219 & 0.0133 & 0.003 \\ 0.0133 & 0.0596 & 0.0983 & 0.056 & 0.0133 \\ 0.0219 & 0.0983 & 0.1621 & 0.0983 & 0.0219 \\ 0.0133 & 0.0596 & 0.0983 & 0.0596 & 0.0133 \\ 0.003 & 0.0133 & 0.0219 & 0.0133 & 0.003 \end{bmatrix} \qquad (10)$$

This filter eliminates the noise effects on the points. Using a larger Gaussian Filter and a greater σ decreases the accuracy of the measurements.

The edges in the image always contain useful information. Generally edge is the boundary of major variation between two parts of an image and there are various methods for edge detection in image processing references.

As described edge detection is defining locus of the image function *f(x,y)* deviations. Here the image is 2D so we use 2 variants and partial differential equations to calculate the deviations. The equation below shows the differential of the function *f(x,y)*.

4

$$G(x,y) = \|\nabla f(x,y)\|$$
$$= \sqrt{\left(\frac{d}{dx}f(x,y)\right)^2 + \left(\frac{d}{dy}f(x,y)\right)^2} \quad (11)$$

The equation shows the gradient of function $f(x,y)$ and the magnitude of the gradient vector shows the deviations of the function $f(x,y)$ in the direction of the gradient vector.

$$\nabla f(x,y) = \left[\frac{\partial f}{\partial x} \quad \frac{\delta f}{\delta y}\right] = [f_x \quad f_y] \quad (12)$$

By thresholding on magnitude of the gradient vector the edges of the image are detected.

Because the magnitude of $f(x,y)$ can't be calculated continuously, it's gradient is not analytically computable. So the gradient is calculated approximately. There are many methods for approximating the gradient of the image which are 2D and their convolutions are calculated in the image matrix. Among these methods *Sobel Mask* is more applicable and has less sensitivity to the disarray of the image.

Equations (13) and (14) show the *Sobel Mask* and how its convolution is calculated.

$$S_y = \begin{bmatrix} -1 & -2 & -1 \\ 0 & 0 & 0 \\ 1 & 2 & 1 \end{bmatrix}, S_x = \begin{bmatrix} -1 & 0 & 1 \\ -2 & 0 & 2 \\ -1 & 0 & 1 \end{bmatrix} \quad (13)$$

$$\begin{aligned} S_x \otimes f(i,j) = & -f(i-1,j-1) \\ & - 2f(i-1,j) \\ & - f(i-1,j+1) \\ & + f(i+1,j-1) \\ & + 2f(i+1,j) + f(i+1,j \\ & +1) \end{aligned} \quad (14)$$

The algorithm used for creating the binary matrix and its schematic is shown in figure 6.
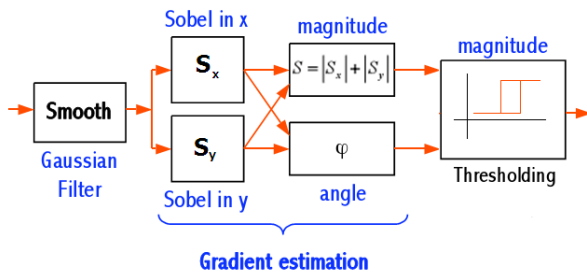

Figure 6 – Schematic steps in creating binary matrix

The general form of the condition applied for creating the binary matrix is shown in the equation (15)

$$B(x,y)$$
$$= \begin{cases} 1 & \text{if } \sqrt{f_x(x,y)^2 + f_y(x,y)^2} > Threshold \\ 0 & else \end{cases} \quad (15)$$

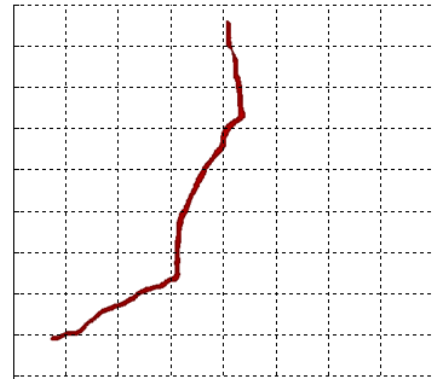Figure 7 shows the final result of image processing.

Figure 7 - The detected edge in the image and the final result of image processing section

This binary image defines the dimensions of points on the laser beam. Now in order to calculate the 3D model of the weld we need to fit a desired curve on these points.

CREATING THE WELD MODEL

Since 1970 useful characteristics and various advantages of *B-Splines* has made them one of the standard tools for representing the curves in every branches of engineering. The result of image processing is a pile of discontinuous data which should be represented in a desired form. B-Spline curve is an appropriate method for representing these points. And fitting a B-Spline is one of the applicable problems in engineering. In this project we have used SDM[1] for fitting B-Spline curves which is one of the most applicable methods of curve fitting.

If we have $n+1$ control points $P0$, $P1$ ... $Pn+1$ and the nodal vector $U = \{u_0, u_1, \ldots, u_m\}$, using base functions of *B-Spline* curves which are shown in equations (16) we can compute a p order *B-Spline* curve as shown in equation (17).

$$N_{i,0}(u) = \begin{cases} 0 & u_i \leq u < u_{i+1} \\ 1 & else \end{cases}$$

$$N_{i,p}(u) = \frac{u - u_i}{u_{i+p} - u_i} N_{i,p-1}(u)$$
$$\quad + \frac{u_{i+p+1} - u}{u_{i+p+1} - u_{i+1}} N_{i+1,p-1}(u)$$
$$(16)$$

$$C(u) = \sum_{i=0}^{n} N_{i,p}(u)P_i \quad (17)$$

There are three major characteristics of base function of *B-Spline* which makes our model suitable for the project:

---

[1] Squared Distance Minimization

1- The curve's order is not dependent on the number of control points.
2- The base functions of *B-Spline* curves are not zero in determinant nodal ranges.
3- We can correct the curve not only by changing the control points but also by changing the nodal vector.

If $n+1$ data points are known, we need two other data to calculate the *B-Spline* which are number of control points $h+1$ and order of the curve p. there is also a relation between these data.

$$n > h \geq P \geq 1 \qquad (18)$$

The curve collides with the start and end point so:

$$D_0 = C(0) = P_0 \quad , \quad D_n = C(1) = P_h \qquad (19)$$

Now the coordinates of $h-1$ control points are unknown which can be calculated using the following equations.

$$C(u) = N_{0,p}(u)D_0 + \left(\sum_{i=1}^{h-1} N_{i,p}(u)P_i\right) + N_{h,p}(u)D_n \qquad (20)$$

And the amounts of the error function can be calculated:

$$f(P_1, \dots, P_{h-1}) = \sum_{k=1}^{n-1}|D_k - C(t_k)|^2 \qquad (21)$$

By assuming f function as the error function, only control points which minimize the amount of f are accepted. By recalculating the difference of a point by its corresponding position on the curve we have:

$$D_k - C(t_k) = \left(D_k - N_{0,p}(t_k)D_0 - N_{h,p}(t_k)D_n\right) - \left(\sum_{i=1}^{h-1} N_{i,p}(t_k)P_i\right) \qquad (22)$$

For simplifying the formulations, Q is defined as follow:

$$Q_k = D_k - N_{0,p}(t_k)D_0 - N_{h,p}(t_k)D_n \qquad (23)$$

By simplifying equation 21 and using equations 22, 23, after differentiation and simplifications a simplified matrix form of the equation are computed:

$$(N^T N)P = Q \qquad (24)$$

N,P,Q are calculated using the following equations:

$$P = \begin{bmatrix} P_1 \\ P_2 \\ \vdots \\ P_{h-1} \end{bmatrix} \quad , \quad Q = \begin{bmatrix} \sum_{k=1}^{n-1} N_{1,p}(t_k)Q_k \\ \sum_{k=1}^{n-1} N_{2,p}(t_k)Q_k \\ \vdots \\ \sum_{k=1}^{n-1} N_{h-1,p}(t_k)Q_k \end{bmatrix} \qquad (25)$$

$$N = \begin{bmatrix} N_{1,p}(t_1) & N_{2,p}(t_1) & \cdots & N_{h-1,p}(t_1) \\ N_{1,p}(t_2) & N_{2,p}(t_2) & \cdots & N_{h-1,p}(t_2) \\ \vdots & \vdots & \ddots & \vdots \\ N_{1,p}(t_{n-1}) & N_{2,p}(t_{n-1}) & \cdots & N_{h-1,p}(t_{n-1}) \end{bmatrix} \qquad (26)$$

Using equations 24, 25, 26 all the data required for interpolating the curve are calculated. Now by inverting $(N^T N)$ and multiplying it by Q, P matrix can be derived. Figure 8 shows the interpolation of a curve on the known points.
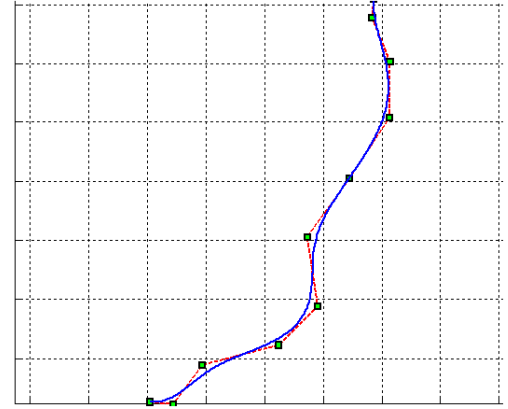
Figure 8 – Interpolated B-Spline on the binary points calculated by edge detection

This curve represents one section of the weld. But for completely modeling the weld we need to calculate dimensions of more sections of the weld. Now we can create a continues model of the weld.

For every desired situation we need a kind of hardware which can capture images from different sections of the weld. Because the main aim of this project was defect detection in the welds used in automobile wheels we designed a rotating system which could easily rotate the part and capture images from different sections of the round weld. Figure 9 shows a weld model generated from 40 sections of the weld.
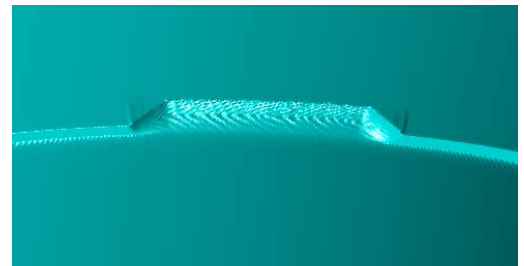
Figure 9 - weld model generated from calculating 40 sections of a weld on automobile wheel

After modeling the weld by comparing it with valid welds we can define weld quality and possible defects created during welding process.

6

DEFECT RECOGNITION

Recognizing weld defects from its external appearance is a fast, simple and low cost process which shows weld quality. Figures 10 and 11 show a valid weld and an incomplete weld with cavity.

Figure 10 - an example of a valid weld on automobile wheel

Figure 11 - an invalid weld with cavity

There are different kinds of exterior defects. In this project the following defects are recognizable.

1. Surveying weld position
2. Surveying weld width and its uniformity
3. Continuity of weld chains
4. Surveying possible holes in the weld
5. Surveying possible porosity in the weld
6. Surveying possible scorch on weld surface

These defects are recognizable by comparing the 3D model generated from the weld and a healthy and valid weld sample. Figures 12 to 14 shows some weld models generated from valid and invalid welds with different defects.
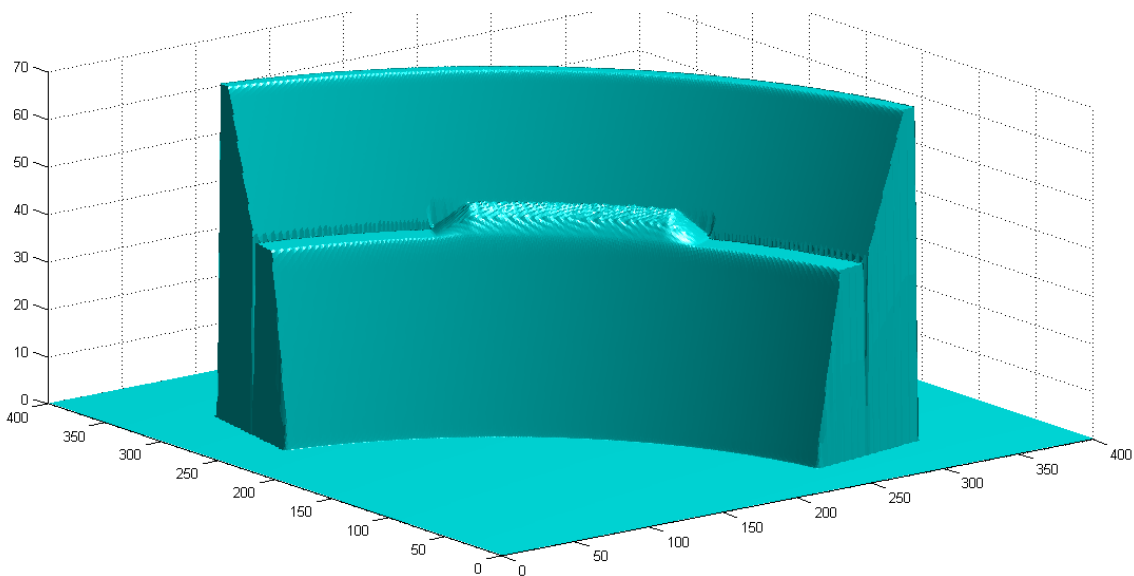

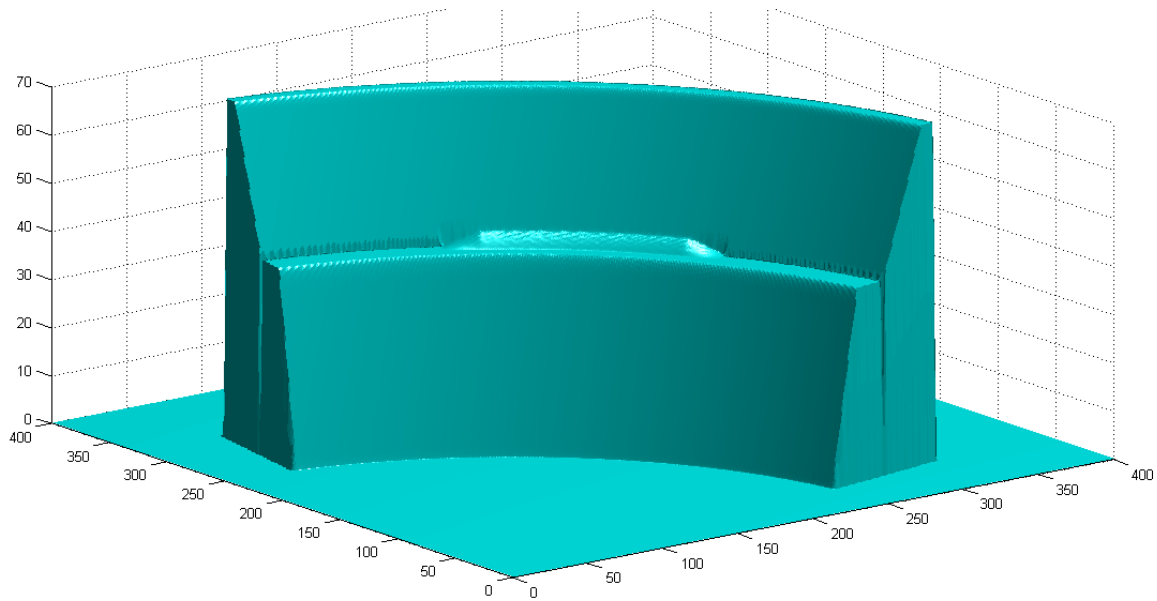Figure 12 - a valid weld model used as reference for defect detection

7

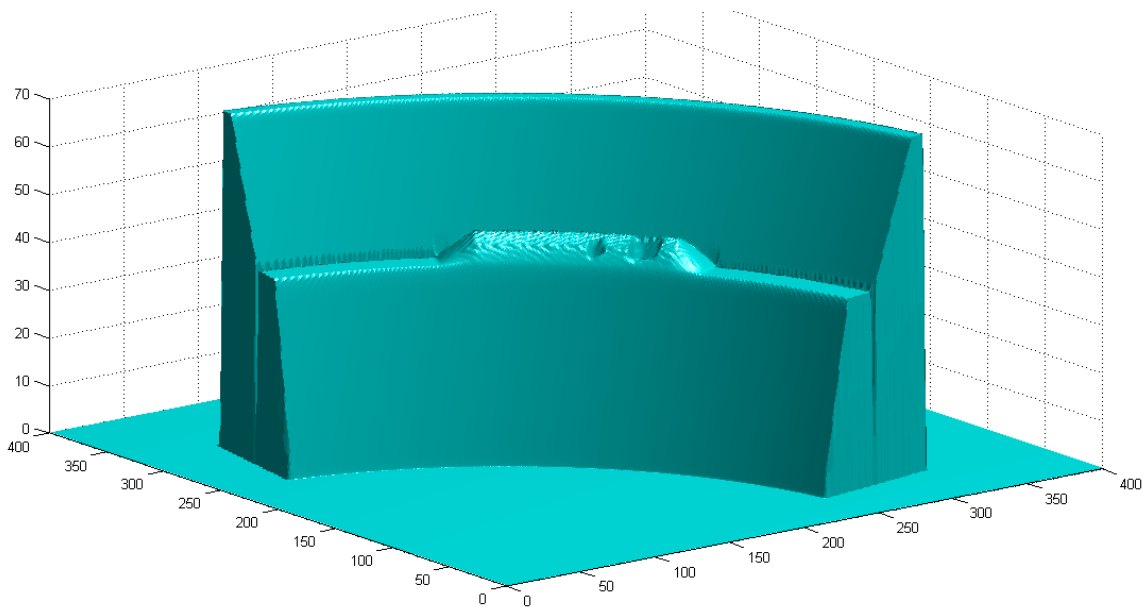Figure 13 - Invalid weld because of miss positioning

Figure 14 - Invalid weld because of cavity occurrence in the middle of the weld

CONCLUSION

The presented article is a new and applicable method for weld quality control based on 3D measurement of weld indentation using modern image processing algorithms and CAD transformations.

The applicability of the method is demonstrated through indentation measurements of a batch of wheel welds obtained from production process in Mashhad Wheel Manufacturing Co. in which defects are detected only by operator's visual tests.

We have examined the potential of the described method by checking the parts, in line with the QC station of the company. All processes were carried out automatically, and the range of the main parameters could be set regarding the

required accuracy for every kind of product, avoiding the need for any external intervention in the process. And we checked the results of our method by the operator's decision in visual test method which in passage of time showed many more advantages of the presented method such as:

Increase in the quality of the products, Decrease in production costs and defect amendments, higher accuracy in decision and opportunity for more accurate adjustments, Decrease of harmful effects on the health of the operators.

AKNOWLEDGEMENTS

REFRENCES

1- Edward GR. Inspection of welded joints. ASM handbook, welding brazing and soldering, vol.6 .MaterialsPark, OH: ASM International 1993. p. 1081–8.

2- Boillot, iean-aul and Noruk, Jeffrey. The Benefits of laser vision in robotic arc welding, American welding society – welding journal, august 2002

3- Abdel-Aziz, Y. I. and Karara, H. M., 1971, Direct linear transformation into object space coordinates in close-range photogrammetry. Proc. Symposium on Close-Range Photogrammetry, Urbana, Illinois, p. 1-18.

4- Tsai, R. Y. , 1987, A versatile camera calibration technique for high-accuracy 3D machine vision metrology using off the-shelf TV cameras and lenses. IEEE Journal of Robotics and Automation RA-3(4): 323-344.

5- Grigorescu C., 2003, Contour Detection and Shape Recognition in Image Analysis, PhD Dissertation, University of Groningen

6- Pottmanna H., Leopoldsedera S., Hofera M., Steinera T. and W. Wang., 2005, Recent advances and applications in CAD, Computer-Aided Design Vol37 P751–766

7- Dierckx P. Curve and surface with splines, Oxford: Clarend Press, 1993.

8- Eck M, Hoppe H. Automatic reconstruction of B-spline Surface arbitrary topological type. In Proceeding of SIGGRAPH 96, 1996. P325-34

9- Murakami K. Image processing for non destructive testing, Weld Int, 1990. Vol 4. P 144-9

10- Kehoe. The detection and evaluation of defects in indusrial ages, Ph.D Thesis, University of Surrey 1990.

11- Matsuyama K. Review on inspection technique for spot welds, Lisbon, 1999.